catalysts

MDPI

Review

Preparation and Electrocatalysis Application of Pure Metallic Aerogel: A Review

Ran Zhang [1] and Yan Zhao [1,2,3,4,*]

[1] Institute of Laser Engineering, Faculty of Materials and Manufacturing, Beijing University of Technology, Beijing 100124, China; s201713003@emails.bjut.edu.cn
[2] Key Laboratory of Trans-scale Laser Manufacturing Technology (Beijing University of Technology), Ministry of Education, Beijing 100124, China
[3] Beijing Engineering Research Center of Laser Technology, Beijing University of Technology, Beijing 100124, China
[4] Beijing Colleges and Universities Engineering Research Center of Advanced Laser Manufacturing, Beijing 100124, China
* Correspondence: zhaoyan@bjut.edu.cn; Tel.: +86-010-67391927

Received: 5 October 2020; Accepted: 23 November 2020; Published: 25 November 2020

Abstract: Nanomaterials are widely used in electrocatalysts due to their quantum size effect and high utilization efficiency. There are two ways to improve the activity of nanoelectrocatalysts: increasing the number of active sites and improving the inherent activity of each catalytic site. The structure of the catalyst itself can be improved by increasing the number of exposed active sites per unit mass. The high porosity and three-dimensional network structure enable aerogels to have the characteristics of a large specific surface area, exposing many active sites and bringing structural stability through the self-supporting nature of aerogels. Thus, by adjusting the compositions of aerogels, the synergetic effect introduced by alloy elements can be utilized to further improve the single-site activity. In this review, we summarized the basic preparation strategy of aerogels and extended it to the preparation of alloys and special structure aerogels. Moreover, through the eight electrocatalysis cases, the outstanding catalytic performances and broad applicability of aerogel electrocatalysts are emphasized. Finally, we predict the future development of pure metallic aerogel electrocatalysts from the perspective of preparation to application.

Keywords: aerogel; electrocatalyst; alloy; 3D network structure; self-supported structure

1. Introduction

The International Union of Pure and Applied Chemistry (IUPAC) defines gel as a "non-fluid colloidal network or polymer network that is expanded throughout its whole volume by a fluid." Since ancient times, hydrogels had been widely investigated and utilized. The types of fluids in the network have been continuously studied [1]. In 1864, Graham et al. found that the water in silica gel can exchange with organic solvents [2]. Although the gel can be dried by liquid evaporation under heating, severe shrinkage will inevitably happen. In 1931, Kistler et al. dried the hydrogels by supercritical fluid extraction to avoid the destruction of the gel structure caused by the surface tension. They proposed the concept of an "aerogel" [3].

Preparation strategies for aerogels have been developed for many years [4]. Hydrolysis and the polycondensation of organic precursors (such as tetramethyl orthosilicate [5], glucose [6], etc.) are traditional methods to obtain aerogels. The limitations in the types and preparation of materials greatly restrict the development of aerogels. In 2004, Mohanan et al. divided the preparation of CdS aerogels into two independent processes: the preparation and gelation of CdS nanoparticles. Firstly,

thiolate-stabilized CdS nanoparticles were prepared by a reverse micelle route, and then CdS hydrogels were obtained by oxidizing surfactants to destabilize the gels. Finally, CdS aerogels with a specific surface area of 242 m^2/g were obtained by CO_2 supercritical drying [7]. The composition and structure of monomers can be tuned, which extends the types of aerogels and provides a new idea for aerogel preparation. Due to the high porosity, high specific surface area, and 3D self-supported structures, aerogels are urgently needed for catalysis. Metal oxide aerogels and carbon aerogels have been widely studied and applied in electrocatalysts [8,9]. However, carbon corrosion and the low conductivity of oxides are the main problems faced by these electrocatalysts in electrocatalytic applications [10]. In 2009, 3D self-supported metal aerogels that exhibit large surface areas and high porosity were first reported by the Eychmüller group, [11]. In 2012, Liu et al. found that the Pd metal aerogels exhibited excellent electrocatalytic activity and stability in ethanol oxidation [12]. Recently, many researchers have devoted themselves to the study of the excellent mechanical and thermal physical properties and related applications of organic aerogels and have made progress [13–15]. As a 3D self-supported network material with excellent electronic conductivity, metal aerogels can completely avoid catalyst structure destruction caused by the decomposition of carbon support at high potential and are widely used as electrocatalyst materials [16]. Furthermore, due to the low content and high price of precious metals, more non-precious metals are also introduced and combined with precious metals to form alloy aerogels for tuning precious metals' electronic structure and reducing costs.

Based on two common preparation methods of aerogels, this article discusses the preparation and formation mechanism of aerogels with tunable compositions and special structures. The analysis of actual cases of electrocatalytic applications shows that the three-dimensional network structure improves the catalytic activity and stability in various electrocatalytic reactions. Moreover, based on the current materials and preparation methods of metal aerogel catalysts, aerogels' future development is expected.

2. Preparation Methods of Aerogels

There are many methods for preparing metal foams with mesh-like porous structures similar to aerogels, including non-sol–gel methods such as dealloying, template, combustion, and the direct freeze-drying method [17–20]. Due to the mild reaction conditions, simple preparation process, excellent composition, and structure control ability, sol–gel methods have always been one of the most promising ways of preparing nanometal foam materials. Next, we will introduce two common sol–gel methods for preparing aerogels as shown in Figure 1.

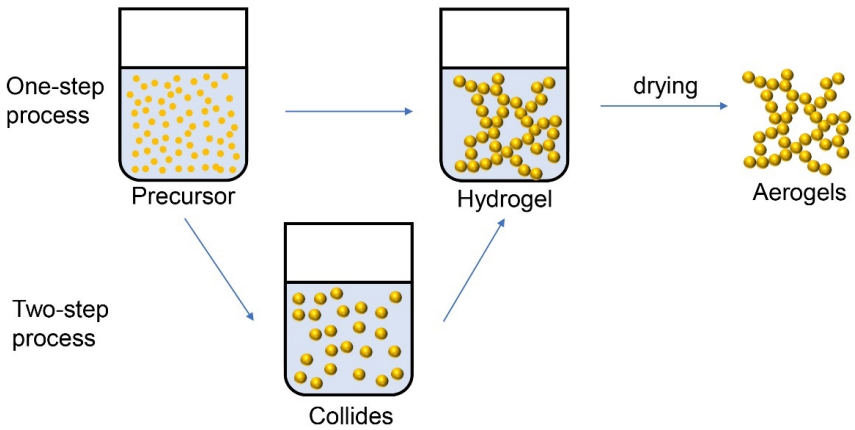

Figure 1. Two aerogel preparation processes.

2.1. Two-Step Process

The two-step process can be divided into two parts. Firstly, stable metal nanoparticle sol can be obtained by reducing precursors. The metal nanoparticles with ligands attached to the surface

can be formed after the stabilizers are ionized or hydrolyzed, which can bring electrostatic repulsion and space repulsion to balance the van der Waals force among particles and ensure colloidal stability. After removing impurities and excess stabilizers by concentrating and reducing the repulsive force of the ligands by the chemical method, the sol is gradually destabilized with the nanoparticles connected. Finally, the hydrogel is formed and precipitated to the bottom of the container. Unlike the traditional sol–gel methods obtained via hydrolyzing and polycondensing molecular precursors, the gel obtained by the self-assembly of high-crystallinity nanoparticles does not need further annealing to ensure the structure's stability [21,22].

Interestingly, the gelation process has little effect on the structure and chemical composition of the monomers. Duan et al. achieved the gelation of gold nanoparticles with different sizes for the first time [23]. Suraj Naskar et al. obtained Pt nanocubes by a facile solvothermal approach firstly. After cleaning the surfactant on the Pt nanocubes, ammonia was added as the initiator to promote the Pt nanocubes gelation [24]. Since the preparation and gelation of monomers are independent, much effort is devoted to regulating the composition and structure of aerogels through a mature monomer synthesis technique. However, because of the more straightforward synthetic step, the current one-step process for preparing aerogels has attracted great attention.

2.2. One-Step Process

Liu et al. pioneered the preparation of Pd aerogels by a one-step process. In the presence of the capping agents (a-, b-, or g-cyclodextrins, CD), $NaBH_4$ was used to reduce K_2PdCl_4, which could promote the self-assembly of Pd-CD nanoparticles. Then, the nanoparticles were dried with supercritical CO_2 to obtain Pd-CD aerogel [12]. The controlling temperature can also achieve the purpose of accelerating the gelation kinetics. Jin et al. added $H_2PtCl_6{\cdot}6H_2O$ and $RhCl_3{\cdot}3H_2O$ to $NaBH_4$ solution at 60 °C; after one minute of vigorous stirring and standing in a water bath at 60 °C for 5 h, black floccule appeared in the solution. After about 8 h, the upper layer solution changed from brown to colorless, and a thin layer of PtRh alloy hydrogel settled on the bottom of the beaker [25].

Compared with the two-step process, the one-step process has advantages in regulating the proportion and composition of materials, but it fails in controlling the microstructure of aerogels. These two kinds of methods have their advantages and are suitable for combining different elements and alloy, core–shell, and hollow architecture, which are widely used in the field of electrocatalysis.

3. Drying Process

In changing from hydrogel to aerogel, it is impossible to directly heat and dry because a strong capillary force will be generated at the gas–liquid interface, resulting in shrinking the gel network in the heating and drying step. This shrinkage will reduce the volume of the dried gel to 1/8 of the initial volume. The resulting gel is a xerogel instead of an aerogel [26].

3.1. Freezing-Drying Method

Vacuum freeze-drying is a method to bypass the triple point and avoid the generation of gas–liquid interfaces, which consists of two main stages. Firstly, the temperature is reduced to below the eutectic point temperature, and the water is frozen into ice to retain the material shape. Next, the ice is directly sublimated to vapor by vacuuming. Freeze-drying can keep part of the gel's 3D network structure, but the freezing step may generate large solvent crystals in the hydrogel structure, which tends to produce macropores and makes it difficult to maintain the fine gel structure [27]. Therefore, rapid freezing is required to reduce the damage to the structure by ice crystal growth. In addition, it is preferable to use a solvent with a lower expansion coefficient. The solvent exchange step can be added before freezing-drying.

3.2. Supercritical Drying Method

The supercritical drying is a method to bypass the critical point and avoid the gas–liquid interface. The supercritical fluid is a fluid whose temperature and pressure are higher than the critical temperature (Tc) and critical pressure (Pc). It has a small viscosity, a large diffusion coefficient as gas, and an excellent dissolving performance as the liquid. This ability can be effectively controlled by adjusting the pressure and temperature. The most important thing is that the supercritical fluid has nearly zero surface tension, which can avoid the capillary force during the phase transition. Finally, in the supercritical state, liquid CO_2 is used to replace the supercritical water. After the pressure is reduced, the CO_2 becomes a gas and is then released, and the fine 3D structure of the aerogel is retained [23].

4. Preparation of Alloy Aerogel

Multi-metallic aerogels can be obtained by simply mixing different metal nanoparticles and co-gelation. Herrmann et al. obtained multi-metallic aerogels Au-Ag, Au-Pt, Ag-Pd, Ag-Pd, Pt-Pd, Au-Ag-Pt, Au-Pt-Pd, Ag-Pt-Pd, and Au-Ag-Pt-Pd by mixing different metal nanoparticle colloids [28]. Although dimers' interparticle coupling can play a role in electrocatalysis, there are fewer application cases in electrocatalysis than alloy aerogels with stronger synergetic effects due to the multi-metallic aerogels' low degree of alloying. Du et al. obtained citrate-stabilized AuPt and AuRh alloy nanoparticles by a reduced mixed precursor at first; then, they added fluoride salt with a strong salting-out effect to induce the gelation of AuPt and AuRh alloy nanoparticles. Compared with multi-metallic aerogels, the coupling between metals in obtained AuPt and AuRh alloy aerogels is further strengthened [29].

Compared with the above two-step process, alloy aerogels' preparation based on the one-step process is more straightforward. It only needs to add precursors with different proportions based on the one-step preparation of aerogel. By controlling the concentration ratio of precursors, Liu et al. can prepare PtPd alloys with different atomic ratios via a one-step reduction with $NaBH_4$ [30]. Wang et al. obtained ternary metallic aerogels by a one-step reduction method. Three types of controllable precursor solutions, H_2PtCl_6, $RuCl_3{\cdot}3H_2O$, and $CuCl_2$, were first mixed and stirred at 60 °C and then reduced by adding $NaBH_4$. After washing at 60 °C for two hours, PtRuCu aerogels were obtained via supercritical drying. By changing the ratio of Pt, Ru, and Cu precursors, PtRuCu alloy hydrogels with different elemental compositions were synthesized, and Cu was found to accelerate the gelation process. As a commonly reported method in alloy aerogels, the one-step process has the characteristics of a simple preparation process and easy control of its components [31].

5. Preparation of Aerogel with Special Structures

For maximizing the activity of the aerogel catalyst, the regulation of the aerogels' structure has been stepwise developed based on 3D porous architectures and different element ratios. Special structures (core–shell and hollow structures) are continuously produced by controlling the monomer nanoparticles in the two-step process. The aerogels obtained by the one-step process can also get a special structure through segregation or postprocessing.

5.1. Core–Shell Structure

Segregation often occurs at the interface of different metallic phases, resulting in the formation of alloy or core–shell structures [32,33]. Laura Kühn and co-workers found that after mixing Au and Ag nanoparticles, Au and Ag were homogeneously distributed in the gel structure obtained by co-gelation, and a large number of alloy phases were formed. However, in the Pd-Pt system, the Pt nanoclusters grew on the Pd skeleton; in the Au-Pd system, the Au-Pd core–shell structure was observed [34]. Zhu et al. synthesized the PdPb@Pb core–shell aerogels in one step. The PdPb hydrogel obtained by adding a reducing agent to the precursor solution will undergo component segregation to generate a Pd thin shell of about three atomic layers on the PdPb core (Figure 2a–f) [35]. The core–shell structure obtained by segregation is formed in the process of nanoparticle melting in the early stage of hydrogel

formation, which has high demands for materials and conditions. Therefore, the in situ growth and galvanic replacement process are the mainstream methods of obtaining core–shell structure aerogels. Shi et al. first mixed $HAuCl_4$ and citrate at room temperature to obtain stable Au nanoclusters; then, they added K_2PtCl_4, Na_2PdCl_4, and ascorbic acid for in situ growth for five minutes to obtain $Au@Pt_3Pd$ trimetallic hydrogel. During the process, the K_2PtCl_4 and Na_2PdCl_4 can promote the further reduction of $HAuCl_4$ and help increase the rate of gold gelation. The gold gel skeleton can provide attachment sites for the precursor to be reduced by ascorbic acid, thereby forming an alloy shell on the gold core [36]. Cai et al. obtained the PdAu@Pt core–shell structure via a galvanic replacement approach. First, PdAu aerogels were obtained through a one-step process. To make the galvanic replacement method more efficient and the shell thinner, the aerogel surface was covered with a Cu monolayer through underpotential deposition, and then Pt precursor was added to obtain a Pt shell by replacing the Cu monolayer. This method can also be used to synthesize PdxM-Pt (M=Ni, Co, Cu) core–shell aerogels [37].

In the galvanic replacement method of obtaining the core–shell structure, a trace amount of metal clusters or atoms attachment on the aerogel can be obtained if the content of the shell element precursor is reduced. Shi et al. used pure metallic aerogel as support and replaced Cu with Pd clusters and Pt atoms on the surface of the AuCu three-dimensional network through the galvanic replacement reaction, respectively. This structure combines the advantages of supported catalyst and aerogel structure in electrocatalysis and has broad applicability [38,39].

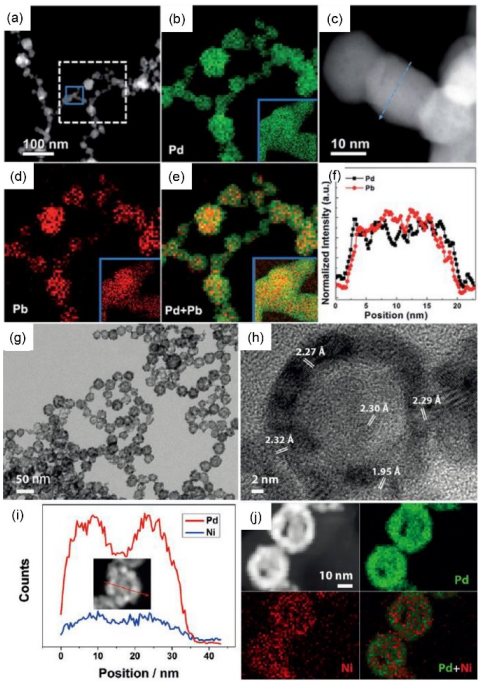

Figure 2. (**a**,**b**,**d**,**e**) scanning transmission electron microscopy- electron energy loss spectroscopy (STEM-EELS) elemental mapping and line scan. (**c**,**f**) results of the Pd_3Pb_1@Pd aerogel [35]. Copyright (2018) Royal Society of Chemistry. (**g**) TEM images of the $Pd_{83}Ni_{17}$ HNS (hollow nanospheres) aerogel at different magnifications. (**h**) high resolution transmission electron microscopy (HR-TEM) characterization of the fused connection and an HNS area of the $Pd_{83}Ni_{17}$ HNS aerogel. (**i**) scanning transmission electron microscopy- energy dispersive spectroscopy (STEMEDX) line-scanning profile and (**j**) high-angle annular dark-field (HAADF) STEM imaging and elemental mapping analysis of Pd and Ni [40]. Copyright (2015) John Wiley and Sons.

5.2. Hollow Structure

The stable three-dimensional network structure of aerogels allows a fast charge transfer and mass diffusion. The hollow architecture further improves the above capabilities, exposes the active sites, and reduces the cost.

The hollow structure often removes the internal structure through the dealloying method or combining the Kirkendall effect and galvanic replacement reaction to obtain higher porosity. In the dealloying method, the core–shell structure is often obtained at first, and then, the internal materials are removed by acid or alkaline dissolution. The Kirkendall effect is an imbalanced inter-diffusion process that occurs at the core/shell interface. The atoms inside continue to dissolve and diffuse to the interface, where a galvanic replacement reaction or reduction reaction occurs at the interface. Liu et al. first reduced $AgNO_3$ with a strong reducing agent to obtain Ag hydrogel; then, they added chloroplatinic acid and got PtAg alloy by the galvanic replacement method. After removing the excess AgCl precursor with HCl and NH_4OH, HNO_3 was used to dissolve the internal silver to obtain a hollow structure. At the same time, partial Ag on the surface was removed, and a large number of holes were distributed on the surface of the hollow nanowire network further to increase the specific surface area [41]. Cai et al. added Pd precursor to the colloids composed of stable Ni nanoparticles, a sacrificial template, to obtain PdNi alloy hollow nanoparticles. After further destabilization, PdNi alloy hydrogels were obtained. PdNi alloy aerogels were prepared by the supercritical drying method (Figure 2g–j) [40]. In addition, combining the galvanic replacement reaction with the Kirkendall effect, Shi et al. reduced the uniformly mixed H_2IrCl_6 and $CuCl_2$ precursors with $NaBH_4$ at 60 °C in one step and obtained alloy aerogels composed of IrxCu alloy nanoshell units. During the above reaction, due to different redox potentials, a core–shell structure composed of an Ir-rich shell and Cu-rich core is gradually formed. Meanwhile, Cu will further replace Ir, and the generated Cu ions flow out to the surface and co-reduced with Ir ions to form an IrCu alloy shell. Cu plays a vital role in the orientated fusion of particles and promotes the formation of a three-dimensional network structure [42].

The core is removed in etching processes or the electric galvanic replacement reaction. Based on the research on hollow nanoparticle materials, a two-step process to obtain hollow structure aerogel materials has also been developed. Ranmohotti et al. first obtained alloy nanoshell aerogels by gelling hollow nanoshells through a two-step process. Firstly, the growth of Ag seeds is controlled by the stepwise addition of precursors to obtain Ag nano-triangles with a hollow structure. Then, the precursor solutions ($HAuCl_4$, K_2PdCl_4, and K_2PtCl_4) were added to obtain hollow AuAg, PdAg, and PtAg alloy nanoshells by the galvanic replacement method. Finally, the colloids is concentrated, and the hydrogel is spontaneously formed with the aid of the salting-out effect of NaCl, and an aerogel composed of alloy hollow nanoparticles is obtained by the supercritical drying method finally [43].

5.3. Other Structures

The nanomaterials obtained by the chemical reduction process often have complex organic ligands. In general, ligands are considered unfavorable for electrocatalysis because they occupy active sites on the surface of catalysts [44,45]. Recent studies suggested that many loosely bound ligands allow the reactants to enter the catalyst surface [46]. The role of ligands in enhancing electrocatalysis has been widely studied [47,48]. Fan et al. introduced the preparation of ultra-small nanoparticles by the laser method into the preparation of aerogels. First, a 1064 nm laser ablation of Au or Pd target in the liquid phase was used to obtain large nanoparticles (>10 nm). Then, the Au colloids were irradiated with a 355 nm laser to obtain stable colloids composed of ultra-small nanoparticles of 4–6 nm. There was no surfactant in the laser ablation and laser irradiation process. Therefore, three kinds of nanoparticles (Au, Pd, and AuPd) without ligands can be obtained. Based on the salting-out effect, $NaBH_4$ was used to gel the above clean nanoparticles. Then, the ligands' effects on the electron density of metal nanoparticles were verified by adding various ligands (trisodium citrate dihydrate, polyvinylpyrrolidone, and cetyltrimethylammonium bromide). The results show that the activity of the AuPd aerogel modified with polyvinylpyrrolidone is 5.3 times that of the commercially available Pd/C

and 1.7 times that of the ligand-free AuPd aerogel during the ethanol oxidation reaction. The presence of organic ligands can promote the transfer of electrons from metals to ligands. The positive potential generated by low-density electrons can accelerate the kinetics of the ethanol oxidation reaction [49].

In addition, due to the oriented attachment of ultra-small particles during the formation process, the particles melt and re-bond, and a large number of defect structures have been found in many reports of aerogel materials, which are conducive for electrocatalysis. Wang et al. prepared PtSn alloy aerogels by the wet chemical method. The high density of defects between the nanoparticles in the aerogel structure improves the intrinsic activity of active sites [50]. Similar defect structures have been discovered in many research studies about aerogels, but no one has quantitatively studied the effect of defects on electrocatalysis.

By tuning the ratios of precursors, the aerogels obtained by the two kinds of methods can form a core–shell or hollow structure under post-treatments such as galvanic replacement, component segregation, in situ growth, and acid corrosion. The above-mentioned post-treatments can also be used to construct special aerogels from the gelation of core–shell or hollow nanoparticles. The high electrochemical active surface area of the above aerogel material is attributed to the three-dimensional network structure with high porosity. The high activities in the fuel oxidation reaction and the oxygen reduction reaction show that the special structure of aerogel considerably promotes intrinsic activity (Table 1).

Table 1. Electrochemical characterization of aerogels.

Materials	Electrolytes	Mass Activities	Specific Activities	ECSAs	Reactions	Ref
$Au@Pt_3Pd$ aerogel	0.1 M $HClO_4$	0.812 A mg_{Pt+Pd}^{-1}	24.3 mA/cm^2	58.7 m^2/g_{Pt+Pd}	ORR	36
PdAu@Pt aerogel	0.1 M $HClO_4$	0.75 A $mg_{noblemetal}^{-1}$	2.53 mA/cm^2	192.3 m^2/g_{Pt}	ORR	37
$Au_2Cu@Pd$ aerogel	1.0 M KOH + 1.0 M ethanol	22.1 A mg_{Pd}^{-1}		89.2 m^2/g_{Pd}	EOR	38
PdNi hollow aerogels	1.0 M NaOH +1.0 M ethanol	3.63 A mg_{Pd}^{-1}	6.54 mA/cm^2	45.2 m^2/g_{Pd}	EOR	41
PVP-modified Au-Pd aerogel	1.0 M KOH + 1.0 M ethanol	6.75 A mg_{Pd}^{-1}		47.7 m^2/g	EOR	49
PtAg hollow nanotubular aerogel	0.1 M $HClO_4$ + 0.5 M HCOOH	237 mA mg_{metal}^{-1}		19.4 m^2/g_{metal}	FOR	40

At present, the preparation of aerogels has begun to be combined with many new preparation technologies, such as laser and 3D printing [49,51], etc. We believe that metal aerogels will be explored from material ratios to structural and will further integrate with a new preparation method in the future. Based on the formation mechanism of aerogels, the gelation time will be further shortened, the porosity of the aerogels will be extended, and aerogels with wider applicability were developed.

6. Application of Aerogels in Electrocatalysis

The above-mentioned various alloy aerogels improve the catalytic activity mainly by adjusting the element types and distribution to tuning the electronic structure of the catalyst, which change the adsorption energy and improve the electrocatalytic performance. In terms of stability, the pure metallic aerogels component without carbon materials avoid carbon corrosion. In addition, the 3D network structure of the aerogel is not prone to agglomeration during the electrocatalytic process, which facilitates mass diffusion and exposes more active sites. The composition and structure ensure the stability of the electrocatalytic process. However, there are still a lot of serious problems in the electrocatalytic detection process. For different materials, there are three methods to detect the electrochemical active surface area (ECSAs): the underpotential deposition of H or Cu, CO stripping method, and the reduction peak detection method. For aerogels with high porosity structure, precisely getting ECSAs is directly related to the specific activity, which is an essential concept of the electrocatalyst. The electrocatalyst involved in various electrochemical reactions (such as oxygen reduction reaction (ORR)) has made a lot of progress in the structure and materials. As a new type of electrocatalyst, pure metallic aerogel needs to find descriptors that can be used to connect the activity and structural characteristics. In addition, the rotating disk electrode (RDE) is one of the main methods for measuring electrocatalytic activity, but it cannot rule out the interference of the actual environment.

Experiments often require more auxiliary ways to verify the electrocatalytic results of aerogel, such as single fuel cell system detection and TEM characterization of the structure before and after the reaction.

The specific performance of pure metallic aerogel in electrocatalysis will be explained in the following section, where we will connect the above characteristics with element types and structural characteristics.

6.1. Cathodic Reduction Reaction

6.1.1. Oxygen Reduction Reaction (ORR)

As efficient energy storage and conversion technology, hydrogen fuel cells have received great attention, but their energy conversion efficiency is limited by the slow oxygen reduction reaction (ORR) kinetics process at the cathode. Therefore, electrocatalysts are needed to increase the reaction rate [52]. Cai et al. combined the underpotential deposition of Cu with the galvanic replacement approach in their work. A layer of Cu was deposited on the PdAu three-dimensional network structure, which is replaced by the Pt in the precursor to get PdAu@Pt aerogel. Adjusting the precursor concentration can obtain core materials with different ratios and even different elements: PdxM (M=Au, Ni, Co, Cu). Among them, $Pd_{20}Au$, $Pd_{10}Au$, Pd_5Au, and Pd_3Au aerogels have high porosity; adsorption isotherms show that the mesopore and macropore structure are widely distributed. Especially, $Pd_{10}Au$ has the lowest density (0.045 g cm^{-3}) and the highest specific surface area (83–105 m^2 g^{-1}). According to the integrated charge generated by H_2 adsorption, the ECSA of $Pd_{20}Au$@Pt aerogel is 192.3 m^2 $g_{Pt}{}^{-1}$, which further verifies its high porosity and high specific surface area. The mass activity of $Pd_{20}Au$@Pt is 5.25 $Amg_{Pt}{}^{-1}$, which is 18.7 times that of commercial Pt/C. After 10,000 cycles in 0.1M $HClO_4$ solution, Pt/C decreased by 27.6%, and the mass activity of $Pd_{20}Au$@Pt aerogel only decreased by 8.2%. In addition, the TEM image shows that the aerogel still maintains a 3D network structure after the stability test, while there is obvious particle aggregation for Pt/C. In addition, due to the elimination of the carbon support, the capacitive current of the aerogel is greatly reduced, and the observed lattice mismatch in the twined crystal and core–shell structure will increase the defect density and further increase the electrocatalytic activity. Based on the three-dimensional network structure, core–shell aerogels can control the types and proportions of the core to tuning the electronic structure and affecting the catalytic activity. With the help of the indirect activity descriptor, the lattice parameter of the core material, the ORR activity of core–shell aerogels can be explained and predicted (Figure 3a) [37]. The special structure brings excellent catalytic activity and stability, and the indirect activity descriptor is due to simple preparation and composition control methods.

The application of aerogel materials in electrocatalysis often requires the use of the electronic and coordination effects brought about by the alloy's special structure to enhance the electrocatalytic activity. Therefore, the ability to quickly build an alloy catalyst with a special structure is a great challenge for aerogels. Shi et al. made simple changes to a common two-process method and quickly prepared $Au@Pt_3Pd$ aerogels with a core–shell structure. The researchers first generated Au(I) by adding $HAuCl_4$ and citrate at room temperature, and then, they added K_2PtCl_4, Na_2PdCl_4, and ascorbic acid (AA) at 35 °C to grow the in situ alloy shell. These two steps have a synergistic effect with each other. Firstly, the Pt(IV) added in the second step can reduce Au(III) to Au(0), accelerating the nucleation of Au, and the salting-out effect promotes the rapid gelation of Au. The entire gelation time is 4 h, which is lower than most of the 6 h gelation time (Table 2).

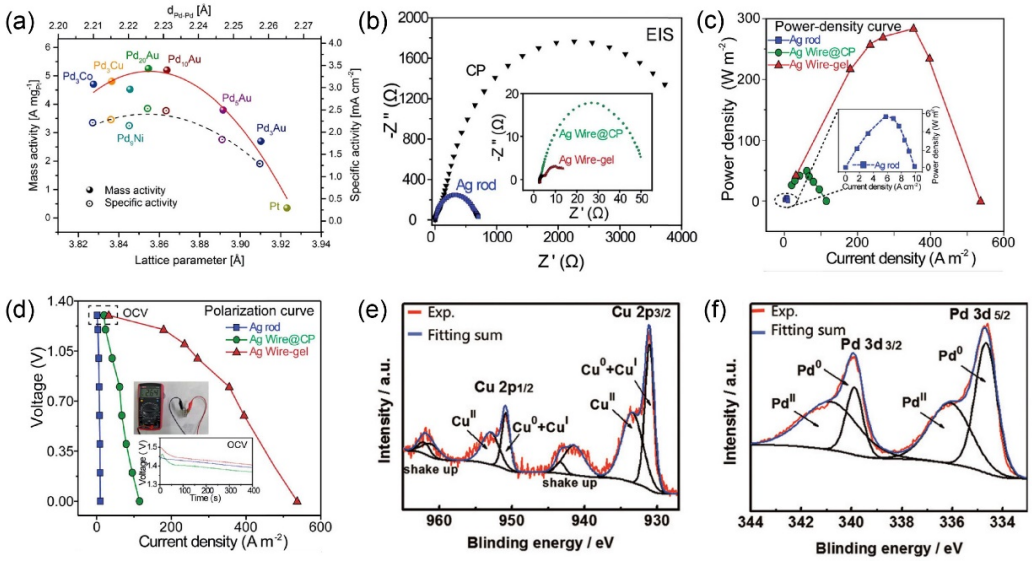

Figure 3. (**a**) The mass and specific activities of the PdxM-Pt core–shell aerogels (M=Au, Ni, Co, Cu) as a function of the lattice parameter and Pd-Pd interatomic distance of the PdxM core aerogels [37]. Copyright (2017) John Wiley and Sons. (**b**) Nyquist plots of the Ag rod (blue) and carbon paper (black). The inset shows the Nyquist plots of the Ag Wire@CP and Ag Wire-gel. (**c**) Power density and (**d**) polarization curves of H_2O_2-fed fuel cells with Ag Wire-gel, Ag Wire@CP, and Ag rod cathodes at different current densities [55]. Copyright (2019) Royal Society of Chemistry. XPS spectra of (**e**) Cu 2p and (**f**) Pd 3d levels of PdCu aerogels [56]. Copyright (2018) John Wiley and Sons.

Table 2. Gel preparation environment commonly used in literature.

Precursors	Reducing Agent	Temperature	Gel Time	Ref
$HAuCl_4$, H_2PtCl_6	$NaBH_4$	60 °C	4 h	[53]
$HAuCl_4$, K_2PtCl_4, Na_2PdCl_4	$NaBH_4$	60 °C	4 h	[36]
H_2IrCl_6 and $CuCl_2$	$NaBH_4$	60 °C	4 h	[42]
H_2PdCl_4 and $AgNO_3$	$NaBH_4$	60 °C	4 h	[54]
H_2PtCl_6, $CuCl_2$ and $RuCl_3$	$NaBH_4$	60 °C	4 h	[31]

Secondly, the generated 3D mesh Au aerogel has a high specific surface area and can provide many attachment sites for the precursors. The synthesized aerogel has excellent catalytic activity, and the half-wave potential (0.897 V) is positively shifted by 30.7 mV compared with commercial Pt/C. The mass activity and specific activity (0.812 A/mg_{Pt+Pd} and 24.3 mA/cm^2) of aerogels are about twice that of commercially available Pt/C. This activity comes from the aerogel interconnected channels, which increases the active site, the mass transfer rate, and the electronic effect of the surface Pt_3Pd, which downshifts the Pt d band. The combination of the three metals promotes the lattice strain and the geometric effect, which reduce the bonding strength of the oxygen-containing intermediate to the Pt surface [36].

6.1.2. H_2O_2 Reduction Reaction (H_2O_2RR)

Liquid H_2O_2 is easier to store and transport and can be used as a substitute for cathode oxidants, such as O_2 or air. At the same time, the fuel cell will exhibit high output voltage and energy density. However, hindered electron transfer and H_2O_2 transport have always been major problems that limit the rate of reduction of H_2O_2 [57]. Yang et al. prepared Ag nanowire hydrogels by a one-step process and obtained Ag nanowire aerogels after freeze-drying. N_2 physisorption isotherms exhibit that the Ag nanowire aerogels have a mesoporous structure of 2–50 nm and a macroporous structure of 50–90 nm, which is consistent with the TEM results. The mesoporous and macroporous structure is beneficial to promote the transfer of reactants, which is essential for the high activity of the H_2O_2

reduction. Ag nanowires with the same average diameter (250 nm) and length (40 μm) attached to the carbon paper (Ag Wire@CP) are of low porosity. The pore volume of Ag Wire@CP is only 1/100 times that of the aerogel structure, and the specific surface area of 8.77 m^2 g^{-1} is much lower than that of the Ag nanowire aerogel (52.86 m^2 g^{-1}). The electrocatalytic results in a three-electrode system show that the exchange current density j_0 of the Ag nanowire gel is 4.4 times more active than Ag Wire@CP. The charge transfer resistance R_{CT} (6.5 Ω) and the ion diffusion resistance R_D (15 Ω) of the Ag nanowire gel are lower than Ag Wire@CP (22.8 Ω and 50 Ω), indicating that metal aerogels are more conducive to electron transport than carbon-supported noble metal catalysts (Figure 3b). To make the electrocatalytic results more convincing, the author assembled the electrocatalyst into the H_2O_2 fuel cell, where the H_2O_2 solution acts as both fuel and oxidant. As shown in Figure 3c, the highest areal power density and current density of the fuel cell with Ag nanowire aerogel as the catalyst are 281 W m^{-2} and 536.6 A m^{-2}, respectively, far exceeding that of the Ag Wire@CP (49.2 W m^{-2} and 115.2 A m^{-2}). Under the same initial open-circuit voltage, with the increase of current density, the drop rate of the open-circuit voltage of the Ag nanowire aerogel is much lower than that of Ag Wire@CP. It still has an open circuit voltage of 1.0 V at a high current density of 200 A m^{-2} (Figure 3d). The detection results in three electrodes and battery systems reflect the excellent properties of aerogels in electron transfer and material transfer compared with nanowires on carbon cloth. The detection results both in the three-electrode system and H_2O_2 fuel cell systems reflect the excellent properties of aerogels in electron transfer and material transfer compared with nanowires on carbon cloth [55].

6.1.3. CO_2 Reduction Reaction (CO_2RR)

CO_2 is the main greenhouse gas, and it is also a cheap, non-toxic C1-rich raw material. Through the CO_2 electrochemical reduction reaction, CO_2 can be converted into chemical products under mild conditions. However, products in the CO_2 electrochemical reaction are more complicated, largely depending on the type and content of materials [58]. Lu et al. first introduced aerogels into the CO_2 electroreduction. As it is easy to control the concentration ratio of the precursor in the preparation method of aerogel, it is also easy to get the element ratio with the highest Faraday efficiency. After mixing H_2PdCl_4 and $CuCl_2$, stirring at 60 °C for one minute, and keeping it at 60 °C for 6 h, the obtained hydrogel is supercritically dried to obtain PdCu bimetallic aerogels. By adjusting the ratio of precursors, the valence states of the constituent elements (Cu^I+Cu^0/Cu^{II} and Pd^0/Pd^{II} values) can be adjusted by tuning the catalytic path and obtain the desired product (Figure 3e,f). Analyzing the product by gas chromatography and NMR spectroscopy shows that the gas product, such as CO, brought by the incomplete reaction is less than 1%, and the liquid product is only methanol. Moreover, due to the excellent structural stability of the aerogel, the current density and Faraday efficiency did not decrease within 24 h. In addition, the TEM and XPS results show that the structure and proportion of the aerogel do not significantly change within 24 h. However, when the hydrogel is dried using a vacuum heating method and freeze-drying method, the three-dimensional structure of the aerogel is destroyed. The Faraday efficiencies of the PdCu bimetallic materials obtained by the two drying methods are 9.6% and 19.6%, respectively, which are far lower than the result of the supercritical drying method (80%). In the process of aerogel preparation, the ratio of the precursor can affect not only the alloy element ratio but also the valence ratio of the elements, thereby tuning the electrocatalytic pathway in the complex electrocatalytic reaction. In addition, by comparing the aerogels after three classes of drying methods, it is easy to find that the high porosity and three-dimensional network structure play important roles in the electrocatalytic results [56].

Zhong et al. added $NaBH_4$ to $HAuCl_4$ and $CuCl_2$, and a hydrogel was formed one hour later. After washing and exchange with ethanol, the surface area of the freeze-dried aerogel reached 27.22 m^2/g. The AuCu aerogels exhibit a superior Faradaic efficiency of ≈100% at an extremely low overpotential of 110 mV and a high CO partial current density of 28.6 mA cm^{-2}. Especially, a very high conversion efficiency (≈13.0%) is achieved when coupling with a Si solar cell to convert solar energy to CO. The characteristics of abundant grain boundaries are the main reason for the above-mentioned catalytic

activity. Since the grain boundary is not conducive to the passage of electrons [59,60], the accumulation of electrons causes the local strong electric field to bring the local high electrolyte concentration, thereby accelerating the surface CO_2 adsorption. In addition, the net-like porous structure is conducive to gas transmission, and the high specific surface area provides a large number of reaction sites. The above characteristics accelerate the conversion efficiency of CO_2 [61].

6.2. Anodic Oxidation Reaction

6.2.1. Methanol/Ethanol Oxidation Reaction (MOR/EOR)

In recent years, direct alcohol fuel cells (DAFC), especially direct methanol/ethanol fuel cells (DMFC/DEFC), have the advantages of simple structure, low price, rich fuel resources, easy transportation, and storage. The methanol/ethanol oxidation reaction involving the transfer of six/twelve electrons that have high energy density but lead to sluggish reaction kinetics. Therefore, it is essential to adjust the composition and ratio to obtain an electrocatalyst with high activity and stability [62–64].

Song et al. added the precursors K_2PtCl_4 and SnC_2O4 to the ethylene glycol (EG) solution containing the surfactant (polyvinylpyrrolidone, PVP) and the reducing agent (phenol). After ultrasonic treatment of the different mixtures for about 0.5 h, it was heated at 160 °C for 5 h, 180 °C for 2 h, and cooled to room temperature to obtain PtSn hydrogels with different ratios. The growth kinetics can be accelerated effectively by increasing the reaction temperature, and the face-centered cubic (fcc) Pt_3Sn phase was obtained gradually (Figure 4a). Comparing the binding energy of pure metal and alloy hydrogels, it is found that the charge can be transferred from Sn to Pt, thereby weakening the adsorption of the intermediate product CO on Pt and exposing more active sites. A large number of kink structures were observed by TEM, indicating that a large number of defects exist. The ECSAs of the Pt_6Sn_3 gel and the commercially available Pt/C electrocatalyst measured by the hydrogen adsorption/desorption curve were 30.90 $m^2\ g^{-1}$ and 64.43 $m^2\ g^{-1}$, respectively. In the ethanol oxidation catalytic reaction, the mass activity and specific activity of Pt_6Sn_3 aerogel are 1.08 mA $mg_{Pt}{}^{-1}$ and 1.40 mA cm^{-2}, respectively, which are 3.5 times and 7.4 times that of the Pt/C electrocatalyst. After 500 cycles, the current density retained 78.04%, while the Pt/C retained only 48.77% (Figure 4b–d). By comparing the results before and after 500 cycles of TEM and EDS, it is found that the Pt_6Sn_3 aerogel maintains the original morphology and composition. However, Pt/C showed serious agglomeration, which is probably the reason for the sudden drop in its catalytic activity. There are also good results for the methanol oxidation catalytic reaction under acidic conditions. The mass activity and specific activity of Pt_6Sn_3 are 3.8 times and 7.8 times that of Pt/C, respectively (Figure 4e). The temperature has a great influence on the structure and phase of the aerogel. The aerogel with the best catalytic activity can be obtained by adjusting the temperature and the precursor. Unlike a large number of noble metal aerogels, the introduction of Sn can reduce the CO poisoning problem of methanol/ethanol fuel cells, and it retains the three-dimensional network structure of the aerogel [65].

The weakness in structural stability, catalytic sites' number, and electrical conductivity of non-noble metals relative to noble metals lead to the poor catalytic stability and activity of non-noble metal electrocatalysts and high starting potential. Amare et al. used the sol–gel methods to obtain a pure non-noble metal aerogel for methanol oxidation firstly. Researchers used $NaBH_4$ to reduce $NiCl_2{\cdot}6H_2O$ and $BiCl_3$ in different proportions to bring a Ni_xBi_y nanowire network structure with a wire diameter of 30–36 nm. After superficial drying, an aerogel was obtained. Ni aerogel doped with trace Bi has excellent catalytic activity (1833.8 A $g_{cat}{}^{-1}$) and still maintains 78% catalytic activity after 12 h. The 3D network structure gives $Ni_{97}Bi_3$ aerogel a high specific surface area of 43.0 $m^2\ g^{-1}$ (Brunauer–Emmett–Teller, BET) and 176.6 $m^2\ g_{cat}{}^{-1}$ (electrochemical active surface area, ECSA), resulting in the most catalytic sites, short diffusion length, and fast proton diffusion rate (2.0×10^{-7} $cm^2\ s^{-1}$) [66].

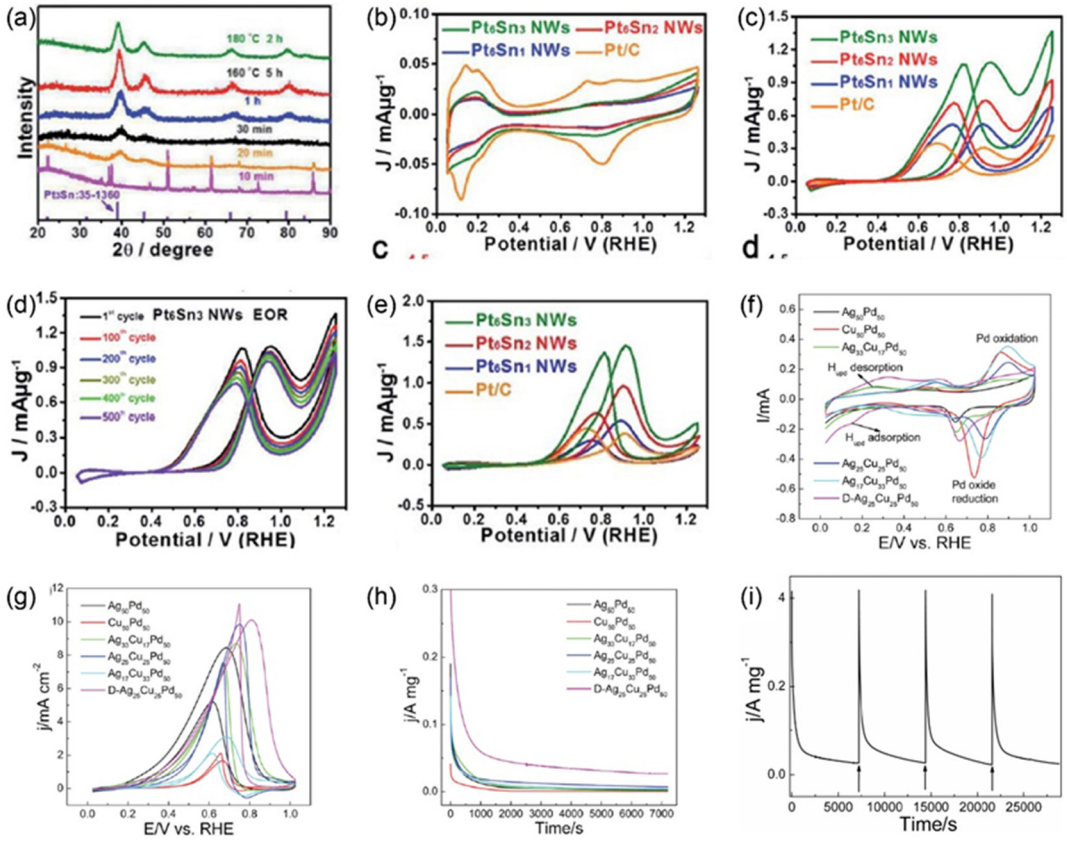

Figure 4. (**a**) Powder x-ray diffraction (PXRD) patterns of the networked Pt_6Sn_3 NWs at different times and temperatures. cyclic voltammetry (CV) curves of different catalysts in (**b**) 0.1 M $HClO_4$ and (**c**) in 0.1 M $HClO_4$ + 0.5 M C_2H_5OH solution with a sweep rate of 50 mV s^{-1}. (**d**) CV curves of the networked Pt_6Sn_3 nanowires (NWs) for the EOR over 500 cycles. (**e**) CV curves in a mixture of 0.1 M $HClO_4$ + 0.5 M CH_3OH [65]. Copyright (2017) Royal Society of Chemistry. (**f**) CV curves obtained in N_2-saturated 1 M KOH solution at a scan rate of 50 mV s^{-1}. (**g**) Electrochemical active surface area (ECSA)-normalized CV curves for the FOR in 1 M KOH + 1 M HCOOK solution at a scan rate of 50 mV s^{-1}. (**h**) Chronoamperometric (CA) curves in 1 M KOH + 1 M HCOOK solution at 0.43 V for 7200 s. (**i**) The long-time stability of the D-$Ag_{25}Cu_{25}Pd_{50}$. The arrows show when the catalyst was reactivated and the electrolyte was exchanged [67]. Copyright (2019) Royal Society of Chemistry.

6.2.2. Formate Oxidation Reactions (FOR)

Formate is easily obtained by reducing CO_2, which is more convenient and safer to store and transport in a solid state [68,69]. Wang et al. synthesized Ag_xPd_{100-x} and $Ag_yCu_{50-y}Pd_{50}$ alloy hydrogels by adding $NaBH_4$ to a controllable precursor. The micro-morphology analysis results show that the wire diameter of D-$Ag_{25}Cu_{25}Pd_{50}$ is about 8 nm, and the ECSA (27.03 m^2 g^{-1}) is much higher than $Ag_yCu_{50-y}Pd_{50}$ (15.01 m^2 g^{-1}), which is also better than the commercial products with ultra-small particles and a high dispersion (Figure 4f). For Pd/C (20.23 m^2 g^{-1}), the high ECSA comes from the rough surface caused by the dissolution of Cu atoms on the surface and the high porosity of the aerogel. The specific activity and mass activity of D-$Ag_{25}Cu_{25}Pd_{50}$ (dealloyed $Ag_yCu_{50-y}Pd_{50}$ aerogel) are 10.10 mA cm^{-2} and 2.73 A $mg_{Pd}{}^{-1}$, respectively, which are 2.73 times and 3.76 times that of Pd/C (Figure 4g). A variety of electrochemical stability test results also reflect the advantages of D-$Ag_{25}Cu_{25}Pd_{50}$. The D-$Ag_{25}Cu_{25}Pd_{50}$ retains 92.40% of the mass activity, and the 3D porous structure is not damaged after the 7200 s chronoamperometric (CA) measurements at 0.43 V while Pd/C only retains 58% of the mass activity. D-$Ag_{25}Cu_{25}Pd_{50}$ maintains good stability and still retains 38.21% of the mass activity after 500 cycles, but Pd/C only has 12.60% of the mass activity after 200 cycles. Figure 4i

shows after three continuous reactivation cycles that the partially deactivated D-$Ag_{25}Cu_{25}Pd_{50}$ can be reactivated after five cycles of 1 M NaOH, which could even undergo another 7200 s CA test in fresh 1 M KOH + 1 M HCOOK solution. It shows that the current decay in the chronoamperometry curve may be caused by the poisoning intermediate formed during the oxidation of formate rather than by the degradation of the catalyst itself, and the 3D network structure was completely retained under long-term operating conditions [67].

7. Mechanism

7.1. Oriented Attachment Mechanism

Both the templates and the uneven distribution of ligands on the particle surface can achieve the purpose of forming a network structure. Some hard templates (such as SiO_2) combined with chemical [70] or electrochemical deposition [71,72] were developed to synthesize nanowire networks in the early stage. However, due to the complicated preparation methods, the removal process is likely to cause environmental and safety issues [73]. The soft template methods, including the microemulsion method [74–77], micelle method [78,79], and bubble template method [80], have been used to synthesize nanowire networks. The bubble template method is widely used in preparing aerogels due to the green and straightforward preparation conditions. Liu et al. obtained the AuPu alloy nanowire network structure by quickly adding $NaBH_4$ solution to the $HAuCl_4$ and H_2PtCl_6 mixed metal precursor at room temperature. Due to the hydrolysis and oxidation of $NaBH_4$, a large number of tiny hydrogen bubbles are generated. The bubble acts as a dynamic template, and the AuPt alloy nuclei reduced by $NaBH_4$ grows on the bubble surface and gap, resulting in a self-supporting interconnected network. The addition rate and concentration of $NaBH_4$ will significantly affect the size, uniformity, and aggregation of H_2 bubbles, thereby affecting the network structure's morphology [80]. What can also prove the advantage of $NaBH_4$ is large particles instead of the previous nanowire structure when Ying et al. used the N_2H_4 instead of $NaBH_4$ [81]. The nanowire network structures in Table 2 are all obtained with $NaBH_4$ addition.

The uneven distribution of the capping ligands on the nanoparticles' surface may also form a 3D gel structure widely used in preparing aerogels. The uneven distribution can occur after the addition of a ligand or the surface ligand gradually removing from the nanoparticle's surface. Yu et al. dissolved palladium(II)-acetylacetonate $Pd(acac)_2$ and $CuSO_4$-$5H_2O$ and polyvinylpyrrolidone (PVP) in ethylene glycol (EG) and synthesized CuPd nanowire networks by heating in one step. Comparing the products' morphologies with a different molecular weight of PVP, they believed that the nanoparticle parts with less surfactant would attach with each other orientally, thus forming a network structure. However, after the molecular weight is reduced, the nanoparticles are severely agglomerated, so the surfactant's precise control has a significant effect on the network's morphology [82]. Ions can also be unevenly distributed on the surface of the particles. Shang et al. found that Br- has selective adsorption on the nanocrystals, and the particles will interact with each other on the bare crystal surface [83].

Gradually removing electrostatic and steric repulsions brought by ligands on the particles' surface is a typical two-step process to obtain aerogels. DLVO theory (Derjaguin and Landau, Verwey and Overbeek) was used to describe the nanoparticles maintaining the force balance in colloids. The total interaction potential (V_T) is expressed as the sum of the electrostatic repulsion potential (V_{elec}), the van der Waals attraction potential (V_{vdW}), the dipolar interaction potential (V_{dipole}), and the charge–dipole interaction potential ($V_{charge\text{-}dipole}$) [84]. However, the DLVO theory can only provide qualitative analysis and is only suitable for solving systems with low concentrations of the order of 0.01 M. During the process of gelation induced by high concentration salt, ions exhibit chemical properties that satisfy the Hofmeister sequence and include the following three mechanisms: Firstly, due to the salting-out effect, the anions and cations ionized by the salt will combine with water to increase the concentration of local nanoparticles. Secondly, the small-sized anions ionized by the salt are more likely to be adsorbed with nanoparticles and further replace the ligands on the nanoparticle's surface.

The adsorption energy can explain the replacement process between the ligands and the nanoparticles. BH^{4-} (E_b = 10.3 kcal mol^{-1}), which has higher binding energies (E_b) to Au nanoparticles, is easier to bind to gold nanoparticles than $citrate^{3-}$ (2.42 kcal mol^{-1}), and BH^{4-} will subsequently degrade to form BO^{2-} (E_b = 0.397 kcal mol^{-1}), which has easy desorption from the surface of gold nanoparticles for the low adsorption energy. Finally, the cations ionized by the initiator will combine with the negatively charged ligands on the surface of the nanoparticles, thereby removing the citrate on the surface of the nanoparticles. Nanoparticles gradually discard the surface charge repulsion and will approach each other under the action of Van der Waals force [85,86]. However, if the ligand removal rate is too fast, the nanoparticles will grow isotropically and agglomerate to form large spherical particles. Slowing down the removal rate of the charged ligands and regulating the long-range charge repulsion force with the short-range van der Waals force will promote nanoparticles' radial growth. According to the lowest energy principle, nanoparticles tend to adhere in the radial direction during the growth process [84].

Although organic ligands' steric repulsion is more complicated, some simple models can qualitatively analyze the instability process. After organics are hydrolyzed, long-chain molecules will anchor on the particle surface, forming a protective shell to ensure nanoparticle colloids' stability. The steric repulsion is mainly caused by the overlapping of the long-chain ligands when particles are close, which discharges the solvent molecules from the interparticle region, resulting in an increasing concentration in the local ligand. When the osmotic pressure increases, the solvent was pushed into the molecular gap. The generated force and the elastic force constitute the balance of the repulsive force and the van der Waals force [87].

The charge and steric repulsions mentioned above are often difficult to separate in experiments. They usually appear in the same ligand (such as trisodium citrate), and the differences in affinity between particles and ligands are used in recent works. Displacing stronger repulsion ligands with weak repulsion ligands can also break the balance between repulsion and the van der Waals force. Fan et al. achieved the purpose of controlling nanoparticles' oriented attachment by replacing ligands on the surface of ultra-small gold nanoparticles. The researchers synthesized ultra-small gold nanoparticles in oleic acid firstly. Oleic acid molecules' long-chain structure balanced the van der Waals force on the gold nanoparticles' surface, which played an excellent stabilizing effect. After the addition of $(NH_4)_2S$, ligand exchange will occur on the gold nanoparticles' surface, since S^{2-} has a stronger affinity of nanoparticles than oleic acid. During the ligand exchange process, the long-chain oleic acid still protects the Au nanoparticles from getting close to each other. However, the replaced S^{2-} can promote the generation of Au-S-Au bonds, connecting the nearby gold nanoparticles. Through further atom diffusion, nanoparticles grow anisotropically and form a three-dimensional network structure [88]. In fact, ionic surfactants on the colloids can also be replaced by the nonionic oligomer surfactants for gelation by heating [89]. There are still other ways to reduce the inter-particle repulsion, such as oxidizing organic ligands on the surface of oxidatively stable nanoparticles [90] and washing the colloidal solution to remove loosely bound stabilizers [91].

7.2. Movement Mechanism

The whole gel process includes the movement process and the bonding process. The movement of particles and clusters mainly consists of the Brownian motion and gravity-driven sedimentation process. Brownian motion is a kind of thermal action; the higher the temperature, the more violent the movement of liquid molecules in the solvent, and the more opportunities for particles to collide with each other. For nanomaterials with or without ligands on the surface, the gelation process can often be accelerated by controlling the temperature [92]. The current one-step aerogel preparation case, which includes the heating step, is shown in Table 2. The Brownian motion and the subsidence process exist simultaneously in the whole process and influence each other. For example, in the process of sedimentation, under the combined action of gravity (G), buoyancy (f), and viscous resistance (F), a concentration gradient will be formed [85]. Due to the long mean free path of a particle in

low-concentration solutions, it is difficult for the particles in Brownian motion to touch each other; gravity-driven sedimentation played a significant role. In a high-concentration part, Brownian motion leads to the rapid formation of a network structure, and the self-weight of the network gel will cause collapse and further precipitation [89].

8. Conclusions and Prospects

Since the metal aerogel was first prepared in 2009, the structure of pure metallic aerogel has undergone considerable development based on traditional aerogels. However, the limited structure, material types, and preparation approaches greatly restrict its application in the field of electrocatalysis. Especially the preparation method, the precursors, and ligands involved in the traditional chemical method require complicated purification steps, which are not conducive to industrial development. Although some new methods have been introduced in the preparation method, due to time reasons, they need considerable development to integrate into aerogel preparation. Secondly, the drying technologies of hydrogel still stay at the supercritical drying many years ago. Although the technical parameters have been improved, the equipment is complicated and the equipment is expensive. As an alternative, the freeze-drying method is more economically viable, but it is hard to protect fine structures. We believe that the development of pure metallic aerogels will mainly accept the following two routes in the future. Firstly, in the preparation of pure metallic aerogels, introducing more non-noble metals into alloy aerogels or even trying to use non-noble-metal aerogels instead of noble metal aerogels is an excellent way to reduce costs. Many synergetic effects are introduced into pure metallic aerogels to expand its application in electrocatalysis; secondly, in terms of industrial production, more nanoparticle preparation, gelation, and the gel drying method are brought in the aerogel preparation to improve the quality and yield of aerogels while reducing costs.

Author Contributions: All authors have contributed to the research work. R.Z. searched the literature, and wrote the main part of the current work; Y.Z. organized, supervised and reviewed the work. Both authors have read and agreed to the published version of the manuscript.

Funding: This work was supported by [the National Natural Science Foundation of China] grant number [NSFC 51475014 and NSFC 11774244].

Conflicts of Interest: The authors declare no conflict of interest.

References

1. Ziegler, C.; Wolf, A.; Liu, W.; Herrmann, A.-K.; Gaponik, N.; Eychmüller, A. Modern Inorganic Aerogels. *Angew. Chem. Int. Ed.* **2017**, *56*, 13200–13221. [CrossRef] [PubMed]
2. Graham, T. XXXV.—On the properties of silicic acid and other analogous colloidal substances. *J. Chem. Soc.* **1864**, *17*, 318–327. [CrossRef]
3. Kistler, S.S. Coherent Expanded Aerogels and Jellies. *Nat. Cell Biol.* **1931**, *127*, 741. [CrossRef]
4. Alwin, S.; Shajan, X.S. Aerogels: Promising nanostructured materials for energy conversion and storage applications. *Mater. Renew. Sustain. Energy* **2020**, *9*, 1–27. [CrossRef]
5. Teichner, S.; Nicolaon, G.; Vicarini, M.; Gardes, G. Inorganic oxide aerogels. *Adv. Colloid Interface Sci.* **1976**, *5*, 245–273. [CrossRef]
6. Fellinger, T.-P.; White, R.J.; Titirici, M.-M.; Antonietti, M. Borax-Mediated Formation of Carbon Aerogels from Glucose. *Adv. Funct. Mater.* **2012**, *22*, 3254–3260. [CrossRef]
7. Mohanan, J.L.; Brock, S.L. A new addition to the aerogel community: Unsupported CdS aerogels with tunable optical properties. *J. Non-Cryst. Solids* **2004**, *350*, 1–8. [CrossRef]
8. Liao, Y.-H.; Chou, J.-C. Preparation and characterization of the titanium dioxide thin films used for pH electrode and procaine drug sensor by sol–gel method. *Mater. Chem. Phys.* **2009**, *114*, 542–548. [CrossRef]
9. Nardecchia, S.; Carriazo, D.; Ferrer, M.L.; Gutiérrez, M.C.; Del Monte, F. Three dimensional macroporous architectures and aerogels built of carbon nanotubes and/or graphene: Synthesis and applications. *Chem. Soc. Rev.* **2013**, *42*, 794–830. [CrossRef]

10. Zhu, C.; Du, D.; Eychmüller, A.; Lin, Y. Engineering Ordered and Nonordered Porous Noble Metal Nanostructures: Synthesis, Assembly, and Their Applications in Electrochemistry. *Chem. Rev.* **2015**, *115*, 8896–8943. [CrossRef]
11. Bigall, N.C.; Herrmann, A.; Vogel, M.; Rose, M.; Simon, P.; Carrillo-Cabrera, W.; Dorfs, D.; Kaskel, S.; Gaponik, N.; Eychmüller, A. Hydrogels and Aerogels from Noble Metal Nanoparticles. *Angew. Chem. Int. Ed.* **2009**, *48*, 9731–9734. [CrossRef]
12. Liu, W.; Herrmann, A.; Geiger, D.; Borchardt, L.; Simon, F.; Kaskel, S.; Gaponik, N.; Eychmüller, A. High-Performance Electrocatalysis on Palladium Aerogels. *Angew. Chem. Int. Ed.* **2012**, *51*, 5743–5747. [CrossRef] [PubMed]
13. Li, Y.; Liu, X.; Nie, X.; Yang, W.; Wang, Y.; Yu, R.; Shui, J. Multifunctional Organic–Inorganic Hybrid Aerogel for Self-Cleaning, Heat-Insulating, and Highly Efficient Microwave Absorbing Material. *Adv. Funct. Mater.* **2019**, *29*, 1807624. [CrossRef]
14. Wong, J.C.; Kaymak, H.; Tingaut, P.; Brunner, S.; Koebel, M.M. Mechanical and thermal properties of nanofibrillated cellulose reinforced silica aerogel composites. *Microporous Mesoporous Mater.* **2015**, *217*, 150–158. [CrossRef]
15. Tang, Y.; Yeo, K.L.; Chen, Y.; Yap, L.W.; Xiong, W.; Cheng, W. Ultralow-density copper nanowire aerogel monoliths with tunable mechanical and electrical properties. *J. Mater. Chem. A* **2013**, *1*, 6723–6726. [CrossRef]
16. Du, R.; Fan, X.; Jin, X.; Hübner, R.; Hu, Y.; Eychmüller, A. Emerging Noble Metal Aerogels: State of the Art and a Look Forward. *Matter* **2019**, *1*, 39–56. [CrossRef]
17. Liu, W.; Herrmann, A.-K.; Bigall, N.C.; Rodriguez, P.; Wen, D.; Oezaslan, M.; Schmidt, T.J.; Gaponik, N.; Eychmüller, A. Noble Metal Aerogels—Synthesis, Characterization, and Application as Electrocatalysts. *Acc. Chem. Res.* **2015**, *48*, 154–162. [CrossRef]
18. Wittstock, A.; Wichmann, A.; Bäumer, M. Nanoporous Gold as a Platform for a Building Block Catalyst. *ACS Catal.* **2012**, *2*, 2199–2215. [CrossRef]
19. Asao, N.; Ishikawa, Y.; Hatakeyama, N.; Menggenbateer; Yamamoto, Y.; Chen, M.; Zhang, W.; Inoue, A. Nanostructured Materials as Catalysts: Nanoporous-Gold-Catalyzed Oxidation of Organosilanes with Water. *Angew. Chem. Int. Ed.* **2010**, *49*, 10093–10095. [CrossRef]
20. Tappan, B.C.; Steiner, S.A.; Luther, E.P. Nanoporous Metal Foams. *Angew. Chem. Int. Ed.* **2010**, *49*, 4544–4565. [CrossRef]
21. Burpo, F.J.; Nagelli, E.A.; Morris, L.A.; McClure, J.P.; Ryu, M.Y.; Palmer, J.L. Direct solution-based reduction synthesis of Au, Pd, and Pt aerogels. *J. Mater. Res.* **2017**, *32*, 4153–4165. [CrossRef]
22. Cai, B.; Sayevich, V.; Gaponik, N.; Eychmüller, A. Emerging Hierarchical Aerogels: Self-Assembly of Metal and Semiconductor Nanocrystals. *Adv. Mater.* **2018**, *30*, e1707518. [CrossRef] [PubMed]
23. Duan, W.; Zhang, P.; XiaHou, Y.; Song, Y.; Bi, C.; Zhan, J.; Du, W.; Huang, L.; Möhwald, H.; Xia, H. Regulating Surface Facets of Metallic Aerogel Electrocatalysts by Size-Dependent Localized Ostwald Ripening. *ACS Appl. Mater. Interfaces* **2018**, *10*, 23081–23093. [CrossRef] [PubMed]
24. Naskar, S.; Freytag, A.; Deutsch, J.; Wendt, N.; Behrens, P.; Köckritz, A.; Bigall, N.C. Porous Aerogels from Shape-Controlled Metal Nanoparticles Directly from Nonpolar Colloidal Solution. *Chem. Mater.* **2017**, *29*, 9208–9217. [CrossRef]
25. Jin, Y.; Chen, F.; Wang, J.; Guo, L.; Jin, T.; Liu, H. Lamellar platinum–rhodium aerogels with superior electrocatalytic performance for both hydrogen oxidation and evolution reaction in alkaline environment. *J. Power Sources* **2019**, *435*. [CrossRef]
26. Pierre, A.C.; Pajonk, G.M. Chemistry of Aerogels and Their Applications. *Chem. Rev.* **2002**, *102*, 4243–4266. [CrossRef]
27. Qiu, L.; Liu, J.Z.; Chang, S.L.; Wu, Y.; Li, D. Biomimetic superelastic graphene-based cellular monoliths. *Nat. Commun.* **2012**, *3*, 1241. [CrossRef]
28. Herrmann, A.-K.; Formanek, P.; Borchardt, L.; Klose, M.; Giebeler, L.; Eckert, J.; Kaskel, S.; Gaponik, N.; Eychmüller, A. Multimetallic Aerogels by Template-Free Self-Assembly of Au, Ag, Pt, and Pd Nanoparticles. *Chem. Mater.* **2013**, *26*, 1074–1083. [CrossRef]
29. Du, R.; Jin, W.; Hübner, R.; Zhou, L.; Hu, Y.; Eychmüller, A. Engineering Multimetallic Aerogels for pH-Universal HER and ORR Electrocatalysis. *Adv. Energy Mater.* **2020**, *10*, 1903857. [CrossRef]

30. Liu, W.; Rodriguez, P.; Borchardt, L.; Foelske, A.; Yuan, J.; Herrmann, A.-K.; Geiger, D.; Zheng, Z.; Kaskel, S.; Gaponik, N.; et al. Bimetallic Aerogels: High-Performance Electrocatalysts for the Oxygen Reduction Reaction. *Angew. Chem. Int. Ed.* **2013**, *52*, 9849–9852. [CrossRef]
31. Wang, H.; Wu, Y.; Luo, X.; Jiao, L.; Wei, X.; Gu, W.; Du, D.; Lin, Y.; Zhu, C. Ternary PtRuCu aerogels for enhanced methanol electrooxidation. *Nanoscale* **2019**, *11*, 10575–10580. [CrossRef] [PubMed]
32. Prabhudev, S.; Bugnet, M.; Zhu, G.-Z.; Bock, C.; Botton, G.A. Surface Segregation of Fe in Pt-Fe Alloy Nanoparticles: Its Precedence and Effect on the Ordered-Phase Evolution during Thermal Annealing. *ChemCatChem* **2015**, *7*, 3655–3664. [CrossRef] [PubMed]
33. Tymoczko, A.; Kamp, M.; Prymak, O.; Rehbock, C.; Jakobi, J.; Schürmann, U.; Kienle, L.; Barcikowski, S. How the crystal structure and phase segregation of Au–Fe alloy nanoparticles are ruled by the molar fraction and size. *Nanoscale* **2018**, *10*, 16434–16437. [CrossRef] [PubMed]
34. Kühn, L.; Herrmann, A.-K.; Rutkowski, B.; Oezaslan, M.; Nachtegaal, M.; Klose, M.; Giebeler, L.; Gaponik, N.; Eckert, J.; Schmidt, T.J.; et al. Alloying Behavior of Self-Assembled Noble Metal Nanoparticles. *Chem. Eur. J.* **2016**, *22*, 13446–13450. [CrossRef]
35. Zhu, C.; Shi, Q.; Fu, S.; Song, J.; Du, D.; Su, D.; Engelhard, M.H.; Yan, X. Core–shell PdPb@Pd aerogels with multiply-twinned intermetallic nanostructures: Facile synthesis with accelerated gelation kinetics and their enhanced electrocatalytic properties. *J. Mater. Chem. A* **2018**, *6*, 7517–7521. [CrossRef]
36. Shi, Q.; Zhu, C.; Li, Y.; Xia, H.; Engelhard, M.H.; Fu, S.; Du, D.; Lin, Y. A Facile Method for Synthesizing Dendritic Core–Shell Structured Ternary Metallic Aerogels and Their Enhanced Electrochemical Performances. *Chem. Mater.* **2016**, *28*, 7928–7934. [CrossRef]
37. Cai, B.; Hübner, R.; Sasaki, K.; Zhang, Y.; Su, D.; Ziegler, C.; Vukmirovic, M.B.; Rellinghaus, B.; Adzic, R.R.; Eychmüller, A. Core-Shell Structuring of Pure Metallic Aerogels towards Highly Efficient Platinum Utilization for the Oxygen Reduction Reaction. *Angew. Chem. Int. Ed.* **2018**, *57*, 2963–2966. [CrossRef]
38. Shi, Q.; Zhu, C.; Tian, M.; Su, D.; Fu, M.; Engelhard, M.H.; Chowdhury, I.; Feng, S.; Du, D.; Lin, Y. Ultrafine Pd ensembles anchored-Au2Cu aerogels boost ethanol electrooxidation. *Nano Energy* **2018**, *53*, 206–212. [CrossRef]
39. Shi, Q.; Zhu, W.; Zhong, H.; Zhu, C.; Tian, H.; Li, J.; Xu, M.; Su, D.; Li, X.; Liu, D.; et al. Highly Dispersed Platinum Atoms on the Surface of AuCu Metallic Aerogels for Enabling H2O2 Production. *ACS Appl. Energy Mater.* **2019**, *2*, 7722–7727. [CrossRef]
40. Cai, B.; Wen, D.; Liu, W.; Herrmann, A.-K.; Benad, A.; Eychmüller, A. Function-Led Design of Aerogels: Self-Assembly of Alloyed PdNi Hollow Nanospheres for Efficient Electrocatalysis. *Angew. Chem. Int. Ed.* **2015**, *54*, 13101–13105. [CrossRef]
41. Liu, W.; Haubold, D.; Rutkowski, B.; Oschatz, M.; Hübner, R.; Werheid, M.; Ziegler, C.; Sonntag, L.; Liu, S.; Zheng, Z.; et al. Self-Supporting Hierarchical Porous PtAg Alloy Nanotubular Aerogels as Highly Active and Durable Electrocatalysts. *Chem. Mater.* **2016**, *28*, 6477–6483. [CrossRef]
42. Shi, Q.; Zhu, C.; Zhong, H.; Su, D.; Li, N.; Engelhard, M.H.; Xia, H.; Zhang, Q.; Feng, S.; Beckman, S.P.; et al. Nanovoid Incorporated IrxCu Metallic Aerogels for Oxygen Evolution Reaction Catalysis. *ACS Energy Lett.* **2018**, *3*, 2038–2044. [CrossRef]
43. Ranmohotti, K.G.S.; Gao, X.; Arachchige, I.U. Salt-Mediated Self-Assembly of Metal Nanoshells into Monolithic Aerogel Frameworks. *Chem. Mater.* **2013**, *25*, 3528–3534. [CrossRef]
44. Lopez-Sanchez, J.A.; Dimitratos, N.; Hammond, C.; Brett, G.L.; Kesavan, L.; White, S.; Miedziak, P.; Tiruvalam, R.; Jenkins, R.L.; Carley, A.F.; et al. Facile removal of stabilizer-ligands from supported gold nanoparticles. *Nat. Chem.* **2011**, *3*, 551–556. [CrossRef] [PubMed]
45. Tran, T.D.; Nguyen, T.M.T.; Le, H.V.; Nguyen, D.N.; Truong, Q.D.; Tran, P.D. Gold nanoparticles as an outstanding catalyst for the hydrogen evolution reaction. *Chem. Commun.* **2018**, *54*, 3363–3366. [CrossRef] [PubMed]
46. Zhang, G.-R.; Xu, B. Surprisingly strong effect of stabilizer on the properties of Au nanoparticles and Pt^Au nanostructures in electrocatalysis. *Nanoscale* **2010**, *2*, 2798–2804. [CrossRef] [PubMed]
47. Xu, G.-R.; Bai, J.; Jiang, J.-X.; Lee, J.; Chen, Y. Polyethyleneimine functionalized platinum superstructures: Enhancing hydrogen evolution performance by morphological and interfacial control. *Chem. Sci.* **2017**, *8*, 8411–8418. [CrossRef]
48. Shan, J.; Zheng, Y.; Shi, B.; Davey, K.; Qiao, S. Regulating Electrocatalysts via Surface and Interface Engineering for Acidic Water Electrooxidation. *ACS Energy Lett.* **2019**, *4*, 2719–2730. [CrossRef]

49. Fan, X.; Zerebecki, S.; Du, R.; Hübner, R.; Marzum, G.; Jiang, G.; Hu, Y.; Barcikowki, S.; Reichenberger, S.; Eychmüller, A. Promoting the Electrocatalytic Performance of Noble Metal Aerogels by Ligand-Directed Modulation. *Angew. Chem. Int. Ed.* **2020**, *59*, 5706–5711. [CrossRef] [PubMed]
50. Wang, C.; Duan, W.; Xing, L.; XiaHou, Y.; Du, W.; Xia, H. Fabrication of Au aerogels with {110}-rich facets by size-dependent surface reconstruction for enzyme-free glucose detection. *J. Mater. Chem. B* **2019**, *7*, 7588–7598. [CrossRef] [PubMed]
51. Yan, P.; Brown, E.; Su, Q.; Li, J.; Wang, J.; Xu, C.; Zhou, C.; Lin, D. 3D Printing Hierarchical Silver Nanowire Aerogel with Highly Compressive Resilience and Tensile Elongation through Tunable Poisson's Ratio. *Small* **2017**, *13*, 1701756. [CrossRef] [PubMed]
52. Wang, J.; Chen, F.; Jin, Y.; Johnston, R.L. Gold-Copper Aerogels with Intriguing Surface Electronic Modulation as Highly Active and Stable Electrocatalysts for Oxygen Reduction and Borohydride Oxidation. *ChemSusChem* **2018**, *11*, 1354–1364. [CrossRef] [PubMed]
53. Cui, C.-H.; Yu, S.-H. Engineering Interface and Surface of Noble Metal Nanoparticle Nanotubes toward Enhanced Catalytic Activity for Fuel Cell Applications. *Acc. Chem. Res.* **2013**, *46*, 1427–1437. [CrossRef] [PubMed]
54. Wang, J.; Chen, F.; Jin, Y.; Guo, L.; Gong, X.; Wang, X.; Johnston, R.L. In situ high-potential-driven surface restructuring of ternary AgPd–Ptdilute aerogels with record-high performance improvement for formate oxidation electrocatalysis. *Nanoscale* **2019**, *11*, 14174–14185. [CrossRef] [PubMed]
55. Yang, Y.; Zhang, H.; Wang, J.; Yang, S.; Liu, T.; Tao, K.; Chang, H. A silver wire aerogel promotes hydrogen peroxide reduction for fuel cells and electrochemical sensors. *J. Mater. Chem. A* **2019**, *7*, 11497–11505. [CrossRef]
56. Lu, L.; Sun, X.; Ma, J.; Yang, D.; Wu, H.; Zhang, B.; Zhang, J.; Han, B. Highly Efficient Electroreduction of CO2 to Methanol on Palladium-Copper Bimetallic Aerogels. *Angew. Chem. Int. Ed.* **2018**, *57*, 14149–14153. [CrossRef]
57. Yang, Y.; Xue, Y.; Huang, F.; Zhang, H.; Tao, K.; Zhang, R.; Shen, Q.; Chang, H. A Facile Microfluidic Hydrogen Peroxide Fuel Cell with High Performance: Electrode Interface and Power-Generation Properties. *ACS Appl. Energy Mater.* **2018**, *1*, 5328–5335. [CrossRef]
58. Cui, M.; Qian, Q.; He, Z.; Ma, J.; Kang, X.; Hu, J.; Liu, Z.; Han, B. Synthesizing Ag Nanoparticles of Small Size on a Hierarchical Porosity Support for the Carboxylative Cyclization of Propargyl Alcohols with CO2under Ambient Conditions. *Chem. A Eur. J.* **2015**, *21*, 15924–15928. [CrossRef]
59. Lee, J.-S.; Anselmi-Tamburini, U.; Munir, Z.A.; Kim, S. Direct Evidence of Electron Accumulation in the Grain Boundary of Yttria-Doped Nanocrystalline Zirconia Ceramics. *Electrochem. Solid-State Lett.* **2006**, *9*, J34. [CrossRef]
60. Zhou, Y.; Sarwat, S.G.; Jung, G.S.; Buehler, M.J.; Bhaskaran, H.; Warner, J.H. Grain Boundaries as Electrical Conduction Channels in Polycrystalline Monolayer WS2. *ACS Appl. Mater. Interfaces* **2019**, *11*, 10189–10197. [CrossRef]
61. Zhong, D.; Zhang, L.; Zhao, Q.; Cheng, D.; Deng, W.; Liu, B.; Zhang, G.; Dong, H.; Yuan, X.; Zhao, Z.; et al. Concentrating and activating carbon dioxide over AuCu aerogel grain boundaries. *J. Chem. Phys.* **2020**, *152*, 204703. [CrossRef] [PubMed]
62. Lin, L.; Zhu, Q.; Xu, A. Anode Catalysts and Cathode Catalysts of Direct Methanol Fuel Cells. *Prog. Chem.* **2015**, *27*, 1147–1157.
63. Yin, P.; Zhou, M.; Chen, J.; Tan, C.; Liu, G.; Ma, Q.; Yun, Q.; Zhang, X.; Cheng, H.; Lu, Q.; et al. Synthesis of Palladium-Based Crystalline@Amorphous Core–Shell Nanoplates for Highly Efficient Ethanol Oxidation. *Adv. Mater.* **2020**, *32*, e2000482. [CrossRef] [PubMed]
64. El Sawy, E.N.; Brueckner, T.M.; Pickup, P.G. Electrochemical Oxidation of Methanol and Ethanol at Rh@Pt and Ru@Pt Catalysts. *J. Electrochem. Soc.* **2020**, *167*, 106507. [CrossRef]
65. Song, P.; Cui, X.; Shao, Q.; Feng, Y.; Zhu, X.; Huang, X. Networked Pt–Sn nanowires as efficient catalysts for alcohol electrooxidation. *J. Mater. Chem. A* **2017**, *5*, 24626–24630. [CrossRef]
66. Dubale, A.A.; Zheng, Y.; Wang, H.; Hübner, R.; Li, Y.; Yang, J.; Zhang, J.; Sethi, N.K.; He, L.; Zheng, Z.; et al. High-Performance Bismuth-Doped Nickel Aerogel Electrocatalyst for the Methanol Oxidation Reaction. *Angew. Chem. Int. Ed.* **2020**, *59*, 13891–13899. [CrossRef]
67. Wang, Q.; Chen, F.; Guo, L.; Jin, T.; Liu, H.; Wang, X.; Gong, X.; Liu, Y. Nanoalloying effects on the catalytic activity of the formate oxidation reaction over AgPd and AgCuPd aerogels. *J. Mater. Chem. A* **2019**, *7*, 16122–16135. [CrossRef]

68. Li, H.-H.; Fu, Q.-Q.; Xu, L.; Ma, S.-Y.; Zheng, Y.-R.; Liu, X.-J.; Yu, S.-H. Highly crystalline PtCu nanotubes with three dimensional molecular accessible and restructured surface for efficient catalysis. *Energy Environ. Sci.* **2017**, *10*, 1751–1756. [CrossRef]
69. Strmcnik, D.; Uchimura, M.; Wang, C.; Subbaraman, R.; Danilovic, N.; Van Der Vliet, D.; Paulikas, A.P.; Stamenkovic, V.R.; Markovic, N.M. Improving the hydrogen oxidation reaction rate by promotion of hydroxyl adsorption. *Nat. Chem.* **2013**, *5*, 300–306. [CrossRef]
70. Shin, H.J.; Ryoo, R.; Liu, Z.; Terasaki, O. Template Synthesis of Asymmetrically Mesostructured Platinum Networks. *J. Am. Chem. Soc.* **2001**, *123*, 1246–1247. [CrossRef]
71. Wang, D.; Kou, R.; Gil, M.P.; Jakobson, H.P.; Tang, J.; Yu, D.; Lu, Y. Templated Synthesis, Characterization, and Sensing Application of Macroscopic Platinum Nanowire Network Electrodes. *J. Nanosci. Nanotechnol.* **2005**, *5*, 1904–1909. [CrossRef] [PubMed]
72. Wang, N.; Luo, H.; Kou, R.; Gil, M.P.; Xiao, S.; Golub, V.; Yang, Z.; Brinker, C.J.; Lu, Y. A General Route to Macroscopic Hierarchical 3D Nanowire Networks. *Angew. Chem. Int. Ed.* **2004**, *43*, 6169–6173. [CrossRef] [PubMed]
73. Song, Y.; Garcia, R.M.; Dorin, R.M.; Wang, H.; Qiu, Y.; Coker, E.N.; Steen, W.A.; Miller, A.J.E.; Shelnutt, J.A. Synthesis of Platinum Nanowire Networks Using a Soft Template. *Nano Lett.* **2007**, *7*, 3650–3655. [CrossRef] [PubMed]
74. Ramanath, G.; D'Arcy-Gall, J.; Maddanimath, T.; Ellis, A.V.; Ganesan, P.G.; Goswami, R.; Kumar, A.; Vijayamohanan, K. Templateless Room-Temperature Assembly of Nanowire Networks from Nanoparticles. *Langmuir* **2004**, *20*, 5583–5587. [CrossRef] [PubMed]
75. Maddanimath, T.; Kumar, A.; D'Arcy-Gall, J.; Ganesan, P.G.; Vijayamohanan, K.; Ramanath, G. Wet-chemical templateless assembly of metal nanowires from nanoparticles. *Chem. Commun.* **2005**, *11*, 1435–1437. [CrossRef] [PubMed]
76. Fang, D.; Wan, L.; Jiang, Q.; Zhang, H.; Tang, X.; Qin, X.; Shao, Z.; Wei, Z.-D. Wavy PtCu alloy nanowire networks with abundant surface defects enhanced oxygen reduction reaction. *Nano Res.* **2019**, *12*, 2766–2773. [CrossRef]
77. Tian, Z.; Zhao, Y.; Wang, S.; Zhou, G.; Zhao, N.; Wong, C.-P. A highly stretchable and conductive composite based on an emulsion-templated silver nanowire aerogel. *J. Mater. Chem. A* **2020**, *8*, 1724–1730. [CrossRef]
78. Yang, D.; Yan, Z.; Li, B.; Higgins, D.C.; Wang, J.; Lv, H.; Chen, Z.; Zhang, C. Highly active and durable Pt–Co nanowire networks catalyst for the oxygen reduction reaction in PEMFCs. *Int. J. Hydrog. Energy* **2016**, *41*, 18592–18601. [CrossRef]
79. Feng, Y.; Bu, L.; Guo, S.; Guo, J.; Huang, X. 3D Platinum-Lead Nanowire Networks as Highly Efficient Ethylene Glycol Oxidation Electrocatalysts. *Small* **2016**, *12*, 4464–4470. [CrossRef] [PubMed]
80. Liu, L.; Chen, L.-X.; Wang, A.-J.; Yuan, J.; Shen, L.; Feng, J.-J. Hydrogen bubbles template-directed synthesis of self-supported AuPt nanowire networks for improved ethanol oxidation and oxygen reduction reactions. *Int. J. Hydrog. Energy* **2016**, *41*, 8871–8880. [CrossRef]
81. Ying, J.; Jiang, G.; Cano, Z.P.; Ma, Z.; Chen, Z. Spontaneous weaving: 3D porous PtCu networks with ultrathin jagged nanowires for highly efficient oxygen reduction reaction. *Appl. Catal. B Environ.* **2018**, *236*, 359–367. [CrossRef]
82. Yu, F.; Zhou, W.; Bellabarba, R.; Tooze, R. One-step synthesis and shape-control of CuPd nanowire networks. *Nanoscale* **2014**, *6*, 1093–1098. [CrossRef] [PubMed]
83. Shang, C.; Guo, Y.; Wang, E. Facile fabrication of PdRuPt nanowire networks with tunable compositions as efficient methanol electrooxidation catalysts. *Nano Res.* **2018**, *11*, 4348–4355. [CrossRef]
84. Zhang, H.; Wang, D. Controlling the Growth of Charged-Nanoparticle Chains through Interparticle Electrostatic Repulsion. *Angew. Chem. Int. Ed.* **2008**, *47*, 3984–3987. [CrossRef] [PubMed]
85. Du, R.; Hu, Y.; Hübner, R.; Joswig, J.-O.; Fan, X.; Schneider, K.; Eychmüller, A. Specific ion effects directed noble metal aerogels: Versatile manipulation for electrocatalysis and beyond. *Sci. Adv.* **2019**, *5*, eaaw4590. [CrossRef]
86. Du, R.; Wang, J.; Wang, Y.; Hübner, R.; Fan, X.; Senkovska, I.; Hu, Y.; Kaskel, S.; Eychmüller, A. Unveiling reductant chemistry in fabricating noble metal aerogels for superior oxygen evolution and ethanol oxidation. *Nat. Commun.* **2020**, *11*, 1590. [CrossRef]
87. Matter, F.; Luna, A.L.; Niederberger, M. From colloidal dispersions to aerogels: How to master nanoparticle gelation. *Nano Today* **2020**, *30*, 100827. [CrossRef]

88. Fan, X.; Cai, B.; Du, R.; Hübner, R.; Georgi, M.; Jiang, G.; Li, L.; Khoshkhoo, M.S.; Sun, H.; Eychmüller, A. Ligand-Exchange-Mediated Fabrication of Gold Aerogels Containing Different Au(I) Content with Peroxidase-like Behavior. *Chem. Mater.* **2019**, *31*, 10094–10099. [CrossRef]
89. Cheng, L.-C.; Sherman, Z.M.; Swan, J.W.; Doyle, P.S. Colloidal Gelation through Thermally Triggered Surfactant Displacement. *Langmuir* **2019**, *35*, 9464–9473. [CrossRef]
90. Gao, X.; Esteves, R.J.; Luong, T.T.H.; Jaini, R.; Arachchige, I.U. Oxidation-Induced Self-Assembly of Ag Nanoshells into Transparent and Opaque Ag Hydrogels and Aerogels. *J. Am. Chem. Soc.* **2014**, *136*, 7993–8002. [CrossRef]
91. Han, X.; Goebl, J.; Lu, Z.; Yin, Y. Role of Salt in the Spontaneous Assembly of Charged Gold Nanoparticles in Ethanol. *Langmuir* **2011**, *27*, 5282–5289. [CrossRef] [PubMed]
92. Du, R.; Jin, X.; Hübner, R.; Fan, X.; Hu, Y.; Eychmüller, A. Engineering Self-Supported Noble Metal Foams Toward Electrocatalysis and Beyond. *Adv. Energy Mater.* **2019**, *10*, 1901945. [CrossRef]